

## Isotropic $^1\text{H}$ and Hyperpolarized $^{129}\text{Xe}$ Gas- and Dissolved-Phase MRI for Longitudinal Evaluation of Lung Cancer

Rohan S Virgincar<sup>1</sup>, Scott H Robertson<sup>2</sup>, Simone Degan<sup>3,4</sup>, Matthew S Freeman<sup>2</sup>, Mu He<sup>5</sup>, and Bastiaan Driehuys<sup>4</sup>

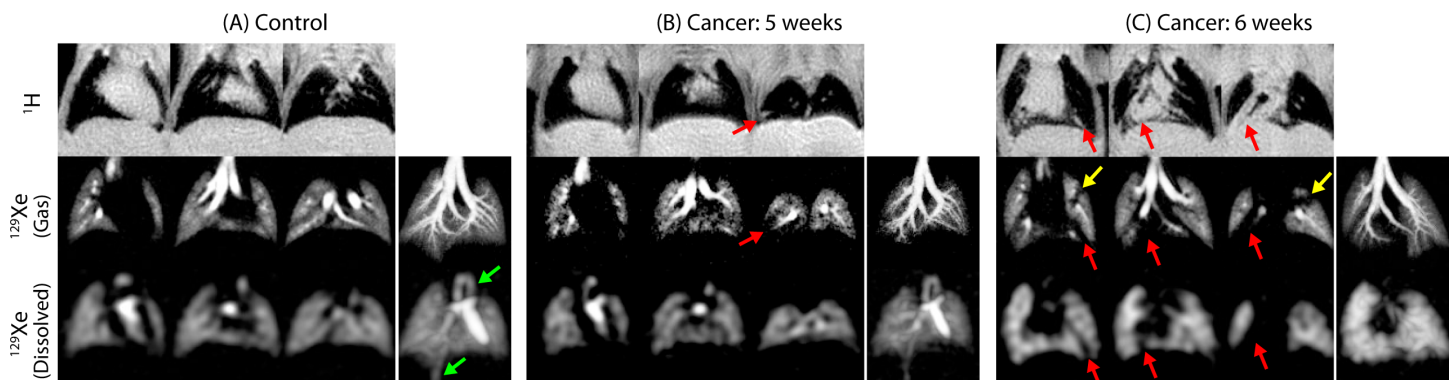
<sup>1</sup>Biomedical Engineering, Duke University, Durham, North Carolina, United States, <sup>2</sup>Medical Physics Graduate Program, Duke University, Durham, North Carolina, United States, <sup>3</sup>Center for Molecular and Biomolecular Imaging, Duke University, Durham, North Carolina, United States, <sup>4</sup>Radiology, Duke University Medical Center, Durham, North Carolina, United States, <sup>5</sup>Electrical and Computer Engineering, Duke University, Durham, North Carolina, United States

**Target Audience:** Hyperpolarized  $^{129}\text{Xe}$  MRI, Pre-clinical functional lung imaging, Lung Cancer

**Purpose:** Hyperpolarized (HP)  $^3\text{He}$  MRI has long been the gold standard for imaging regional ventilation in mouse models of disease<sup>1</sup>. However, the constriction of  $^3\text{He}$  supply has forced a transition to  $^{129}\text{Xe}$  MRI. Moreover,  $^{129}\text{Xe}$  solubility and chemical shift provide a means to add 3D imaging of regional gas-exchange. However, with the exception of notable progress by Fujiwara and coworkers<sup>2</sup>, progress in HP  $^{129}\text{Xe}$  MR imaging of mice has been relatively slow. Thus, there is a need to improve the quality of both  $^{129}\text{Xe}$  ventilation and gas-exchange MRI in mice, which we sought to do by increasing polarization and optimizing 3D radial reconstruction. As a first test of this capability, we have imaged structural and functional alterations in a mouse model of lung cancer longitudinally.

**Methods:** 6-week-old male BALB/c mice (n = 11, ~18 g) were intravenously injected with ~50,000 4T1-GFP breast cancer cells known to create lung tumors over a period of 2-6 weeks. Prior to MRI, animals were anesthetized and intubated orally. They were then ventilated on an HP gas-compatible ventilator with a tidal volume of 0.2 ml (25% O<sub>2</sub>, 75% N<sub>2</sub>/HP  $^{129}\text{Xe}$  polarized to 20%), and imaged in a quadrature  $^{129}\text{Xe}$  coil at 2 T. Mice underwent respiratory-gated  $^{129}\text{Xe}$  gas-phase imaging (3D radial MRI, 132- $\mu\text{s}$  hard-pulse, 2501 views, FOV = 2 cm, Matrix = 128<sup>3</sup>,  $\alpha$  = 30°, TR/TE = 10/0.384 ms, 5 views per breath).  $^{129}\text{Xe}$  dissolved-phase images were acquired with transmit/receive frequency increased by 4660 Hz (selective 1.2-ms 3-lobe sinc pulse, 2001 views, FOV = 4 cm, Matrix = 128<sup>3</sup>,  $\alpha$  = 30°, TR/TE = 50/1.2 ms, 4 views per breath).  $^1\text{H}$  MRI was also conducted for anatomical reference and to visualize tumors (slab-selective 0.5-ms sinc pulse, 51471 views, FOV = 4 cm, Matrix = 256<sup>3</sup>,  $\alpha$  = 15°, TR/TE = 8/2 ms, 20 views per breath). All 3D radial images were reconstructed using optimized 3D gridding<sup>3</sup>. 3-4 animals were scanned every week from 2-6 weeks post-injection of cells. Following each set of scans, the animals were weaned off the ventilator and returned to the cage. Animals were scanned up to 3 times before being sacrificed for H&E histology to estimate the tumor burden and validate imaging findings.

**Results:** Each week, successful survival studies generated isotropic, high-resolution ( $^1\text{H}$ : 156  $\mu\text{m}$ ,  $^{129}\text{Xe}$  gas: 156  $\mu\text{m}$ ;  $^{129}\text{Xe}$  dissolved: 312  $\mu\text{m}$ ) images with high  $^{129}\text{Xe}$  SNR in the parenchyma (gas: 14, dissolved: 23). The figure shows  $^1\text{H}$  and HP  $^{129}\text{Xe}$  MR images of an example control mouse (A), and tumor bearing mouse 5 weeks post- (B) and again at 6 weeks (C) post-instillation. The control mouse exhibits a normal thoracic cavity, and homogeneous, unimpaired ventilation. The dissolved-phase intensity closely matches ventilation distribution, and clearly highlights downstream magnetization in the left heart, aortic arch and descending aorta (Fig. A, green arrows). The cancer animal shows minor defects in both ventilation and gas-exchange at week 5 that escalates at week 6, as both become increasingly impaired near tumors (Figs. B, C, red arrows). In some cancer animals, hyperintensity was noted in portions of the dissolved-phase  $^{129}\text{Xe}$  images, but this could not be definitively associated with tumor presence.



**Discussion and Conclusion:** The quality of  $^{129}\text{Xe}$  mouse MRI now rivals that of  $^3\text{He}$ , and reveals functional impairment associated with metastases formed as early as 4 weeks post-injection of cancer cells. The size and location of defects in  $^{129}\text{Xe}$  images were mostly well-matched with metastases seen on  $^1\text{H}$  MRI, although in several instances  $^{129}\text{Xe}$  ventilation impairment preceded  $^1\text{H}$  MRI changes (Fig. C, yellow arrows). This powerful, non-invasive structural/functional imaging capability is readily applicable to study the progression of a variety of lung disorders, and their responses to therapy.

**Acknowledgements:** NCI R01-CA-142842 and P41 EB015897

**References:** [1] Thomas et al., NMR Biomed. 2009; 22: 502–515; [2] Iguchi et al., Magn. Reson. Med. 70:207–215 (2013); [3] Robertson et al, submitted to ISMRM 2015